Mid-Infrared Images of the Circumstellar Dust Around α Scorpii

K. A. Marsh

Infrared Processing and Analysis Center, Caltech 100-22, Pasadena, CA 91125

E. E. Bloemhof

Caltech 105-24, Pasadena, CA 91125

D.W. Koerner

University of Pennsylvania, 4N14 DRL, 209 South 33rd Street, Philadelphia, PA 19103-6396

and

M.E. Ressler

Jet Propulsion Laboratory, California Institute of Technology, 4800 Oak Grove Drive, Pasadena, CA 91109

Received _____; accepted _____

To be submitted to ApJ Letters

ABSTRACT

We present the first mid-infrared images of the circumstellar dust distribution around the supergiant star α Scorpii. Our observations were made at wavelengths of 12.5 and 20.8 μm using the MIRLIN focal-plane array camera on the Keck II 10-m telescope, with spatial resolution (λ/D) of 0.″29 and 0.″48 at the two wavelengths, respectively. Our deconvolved images, which provide a resolution enhancement of approximately a factor of two, show that the dust shell previously detected in 1-dimensional scans is actually highly nonuniform. Specifically, the shell is now seen to be concentrated largely into 3 discrete clumps, and there is evidence of a more recent ejection which has left a central concentration of dust within about 0.″3 from the star.

Subject headings: infrared: stars — stars: circumstellar matter — stars: individual (α Scorpii) — stars: late-type

1. Introduction

The study of mass loss from supergiants is of interest not only for our understanding of that phase of stellar evolution, but also because such mass loss is a dominant contributor to the enrichment of the interstellar medium. At this time, however, the details of the mass loss process are poorly understood. Possible scenarios involve the ejection of gas from the stellar surface by some mechanism related either to pulsation (Smith et al. 1995) or convection (Schwarzschild 1975), followed by dust formation after the gas has cooled sufficiently (Tuthill et al. 1997). The dust is then blown off by radiation pressure and carries gas with it due to viscous drag, resulting in a stellar wind.

A well-known example of a mass-losing supergiant is the primary component of α Sco (M1.5Iab), which, at a distance of 180 pc (Snow et al. 1987), is close enough for detailed study. Although the system contains a B2.5V secondary, the separation (420 AU—Bernat 1977) is sufficiently large that stellar evolution has probably proceeded independently for the two components.

One-dimensional scans of α Sco at 11 μm wavelength, made in 1985 by Bloemhof & Danen 1995 have suggested a dust shell with an inner radius of $0\farcs6$ (110 AU), under the assumption of spherical symmetry. Observations made using a two-element interferometer at 11.15 μm during 1989–1990 (Danchi et al. 1994) were consistent with this interpretation, and confirmed the lack of dust within about $1''$ from the star. It was not clear from all these observations, however, whether the dust formation is steady-state or episodic. Our recent mid-infrared observations shed some light on this question, and provide further constraints on the mass loss process. We now present those observations.

2. Observations

Our observations of α Sco were made during 1998 June 13, 03:02–03:15 UT and June 14, 01:32–01:51 UT using JPL's mid-infrared camera MIRLIN on the Keck II telescope, at wavelengths of 12.5 and 20.8 μm, with corresponding bandwidths of 1.2 and 1.7 μm respectively. The detector consisted of a 128 × 128 Si:As BIB focal-plane array with a plate scale of 0.″138 per pixel. The effective aperture of the telescope was limited to approximately 9 m by a pupil stop in the camera, giving diffraction-limited resolution (λ/D) of 0.″29 and 0.″48 at 12.5 μm and 20.8 μm, respectively. The air mass was in the range 1.46–1.48 for both of the observation periods. The chopping/nodding technique was used, whereby the secondary mirror was chopped north-south at a rate of 4 Hz and a throw of 5″, and the telescope itself was nodded east-west by 5″at time intervals of approximately 50 s. For each nod, the four raw images (two chop positions at each of two telescope positions) were combined to produce a sky-subtracted image corresponding to a net on-source integration time of 8 s. The individual sky-subtracted images at each wavelength were then combined using the shift-and-add technique, which involved estimating the positions of source peaks using a matched filter whose kernel was derived from the nominal point spread function (PSF). Total integration times on June 13 were 64 and 96 s at 12.5 and 20.8 μm, respectively, and on June 14 the integration time was 160 s (20.8 μm only).

The original intent of these observations was to provide calibration of the PSF for our program of Herbig Ae stars and related objects, but it became apparent during the data reduction that this object was highly extended. Fortunately, a sufficient number of unresolved sources was observed that a reasonable calibration could still be made of our program stars as well as α Sco. The calibrator stars were chosen for their match to α Sco with respect to air mass, and consisted of HD 120323 (M4.5III), HD 167036 (K2III), and β And (M0III).

During the shifting and adding process for both α Sco and the calibrators, explicit account was taken of the image rotation which occurred by virtue of the alt-az telescope mount. This involved a rotational alignment of the individual α Sco images with respect to the north-south direction before shifting-and-adding, and corresponding rotations of the calibrator images to ensure alignment with respect to the telescope diffraction pattern.

Shift-and-add images of α Sco at the two wavelengths are shown in Figure 1. Also shown are the corresponding PSFs, derived from observations of HD 120323 and HD 167036 at 12.5 μm, and β And at 20.8 μm.

Flux calibration of the images yielded total flux densities of 1530 ± 100 and 790 ± 110 Jy at 12.5 and 20.8 μm, respectively, using a $4''.4$ square aperture. These values are consistent with previous estimates, for example: at 12.5 μm, the data of Monnier et al. (1998) show a variation between approximately 1050 and 2100 Jy, while the Q magnitude quoted by Abbot et al. (1984) would imply a 20.8 μm flux of 715 Jy based on the MIRLIN Q3 filter response.

3. Analysis and Results

A comparison between the raw images and PSFs in Figure 1 clearly indicates the presence of some extended structure around α Sco. The spatial extendedness is even more apparent in the profile plots of Figure 2, which show east-west slices through α Sco and comparison stars at the two wavelengths. The comparison stars on this Figure consist of unresolved calibrators (HD 167036, HD 145206, and β And) and nearly-unresolved program stars (HD 150193 and HD 144432).

In order to be able to examine the extended structure without contamination from the bright central star, the estimated photospheric contribution of the latter was subtracted

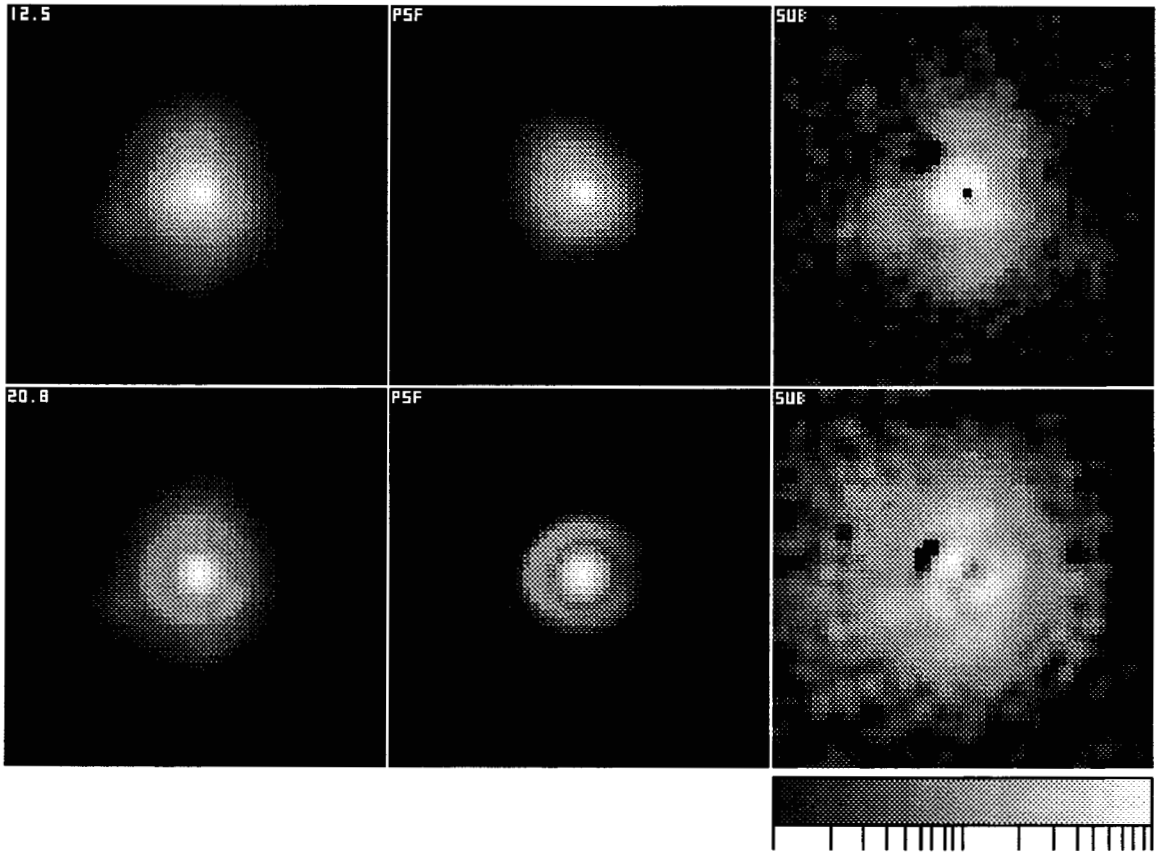

Fig. 1.— Left-hand column: Observed (shift-and-add) images of α Sco at wavelengths of 12.5 and 20.8 μm. Middle column: Corresponding PSFs, derived from observations of HD 120323 and HD 167036 at 12.5 μm, and β And at 20.8 μm. Right-hand column: The result of subtracting the estimated contribution of the stellar photosphere from the observed images shown at the far left. All images are presented on a logarithmic intensity scale of 2 decades, and consist of 48 $\times$ 48 pixels, corresponding to a field of view of approximately 6.″6.

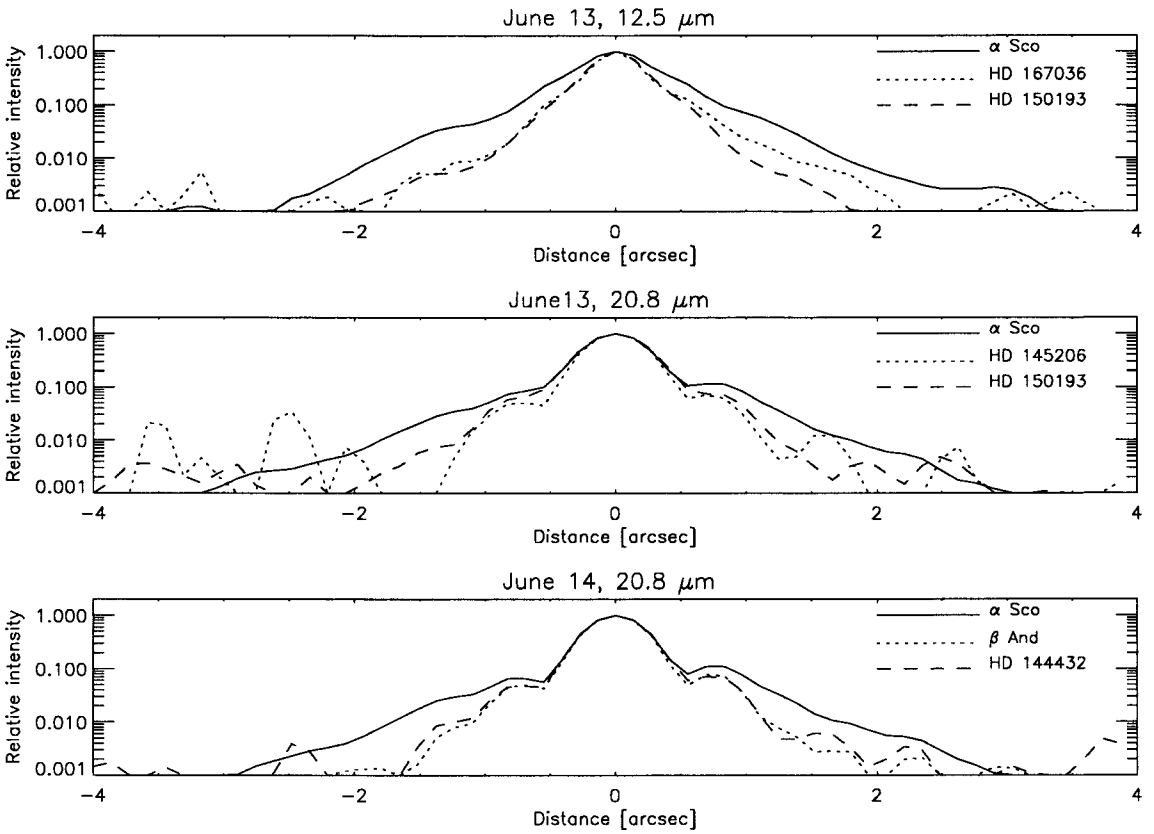

Fig. 2.— East-west slices through the shift-and-add images of α Sco and comparison stars.

from the flux-calibrated images. Our first attempt at this subtraction was based on the interferometric observations of the stellar disk at 11.15 μm, from Bester et al. (1996), which yielded a stellar diameter of 44.0 mas and an effective temperature of 2675 K, implying photospheric fluxes of 1271 and 503 Jy at 12.5 and 20.8 μm after allowance for interstellar attenuation; the latter was taken as 0.941, following Bester el al. Unfortunately, the resulting subtracted image at 12.5 μm showed large negative values in the vicinity of the star, indicating oversubtraction. The negative values were much larger than could be accounted for by errors in the flux calibration or by the stellar disk parameters of Bester et al. (1996), which suggests that the photospheric flux had decreased substantially during the interval 1990–1998.

It was therefore necessary to regard the photospheric flux as an unknown, and to estimate it internally in order to be able to subtract its contribution. For this purpose we derived a maximum likelihood solution to the parameters of a central point source in the presence of an unknown positive background, which corresponded essentially to subtracting the largest possible central point source without producing unreasonable negative residuals. We thereby obtained estimated photospheric fluxes of 960 ± 60 Jy and 540 ± 70 Jy at 12.5 μm and 20.8 μm, respectively, corresponding to factors of 0.75 ± 0.05 and 1.07 ± 0.14 with respect to the values predicted by the Bester et al. parameters. Comparing these results with the behavior of total flux, we find that at 12.5 μm, the fractional decrease in photospheric flux is consistent with the ratio of 0.73 by which the total flux has decreased since the time of the Bester et al. observations. Such variations in photospheric flux are not unexpected, since α Sco is known to be an optical variable, and interferometric observations by Bester et al. have provided direct evidence of mid-infrared photospheric variability in the case of α Her, an object similar in many ways to α Sco. After subtracting the estimated photospheric contribution of the central star at each wavelength on the above basis, we obtained the two images shown in the right-hand column of Figure 1.

The photosphere-subtracted images at the two wavelengths were then deconvolved using the Richardson-Lucy algorithm (Richardson 1972, Lucy 1974) and the results are shown in Figure 3. The images are presented on a 1.5-decade logarithmic scale normalized to peak intensities of 1837 Jy arcsec^{-2} and 361 Jy arcsec^{-2} at 12.5 and 20.8 μm, respectively. These intensities correspond to peak brightness temperatures of 207 K and 122 K, respectively.

In order to investigate the possible effects of PSF error, the images were reprocessed using different PSFs. For this purpose, we used observations of two of our program stars, both of which had been examined for evidence of extended structure and produced negative results. At 12.5 μm, we used δ Cas, a nearby A5III-IV star with a small $\sim$ 10% N-band excess due to a diffuse ($\sim$ 2″) debris disk (Walker & Wolstencroft 1988) which was not detected by our observations. At 20.8 μm, we used HD 144432, an A9/F0V star with a compact debris disk whose inferred diameter (from a fit to the spectral energy distribution) is 0.″09 (Walker & Wolstencroft 1988). Its close proximity to α Sco in the sky makes it a useful PSF calibrator for the present observations. On this basis, we redid the subtraction of the α Sco stellar photosphere at the two wavelengths, and also the deconvolutions, and the results are shown in panels (a) and (b) of Figure 4. The close similarities with the images in Figure 3 provide confidence in the results of the processing.

An additional check on the fidelity of the subtracted/deconvolved images was provided by comparing the 20.8 μm results from the two different days, and the results are shown in panels (c) and (d) of Figure 4. In obtaining these results, it was necessary to use the same PSF for both days (β And from June 14) since there was insufficient S/N in the calibrator observations on June 13 at this wavelength. However, the similarity of the two images indicates that their morphology is not a result of artifacts associated with the α Sco observations.

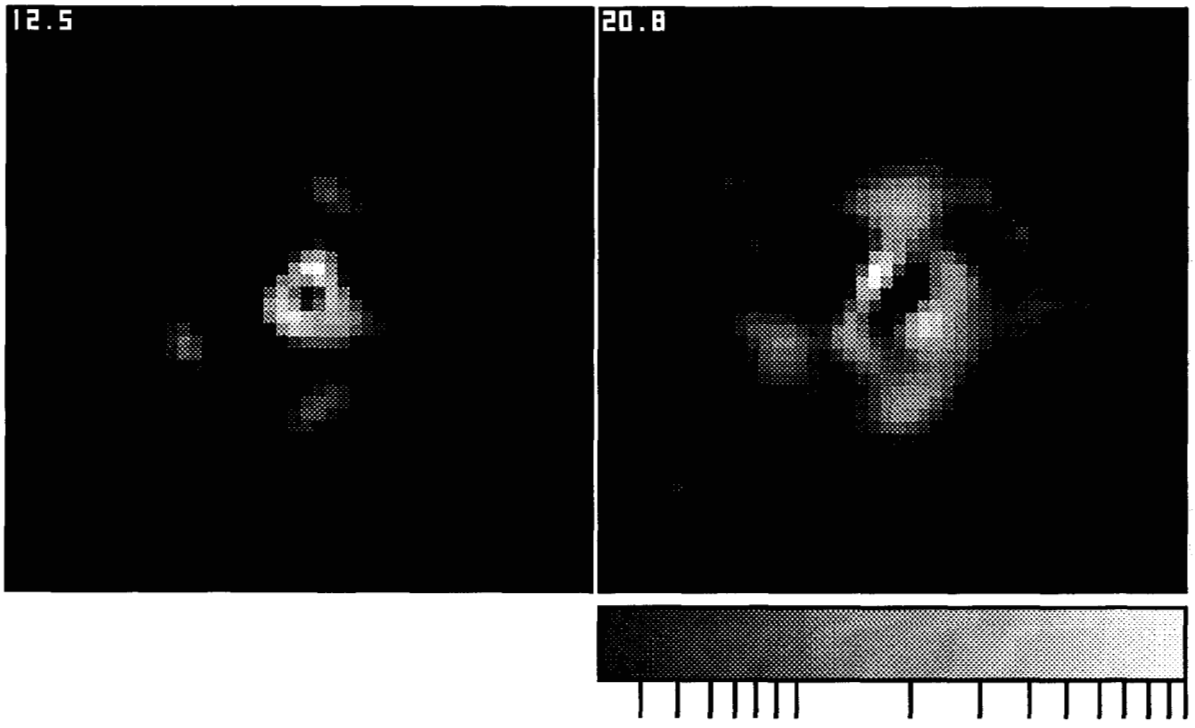

Fig. 3.— Deconvolved images of α Sco after subtracting the estimated contribution of the stellar photosphere at each wavelength. The wavelength in μm is indicated at the top left of each image. The images are presented on a 1.5-decade logarithmic scale, and have the same field of view as for Figure 1, i.e., 6.″6.

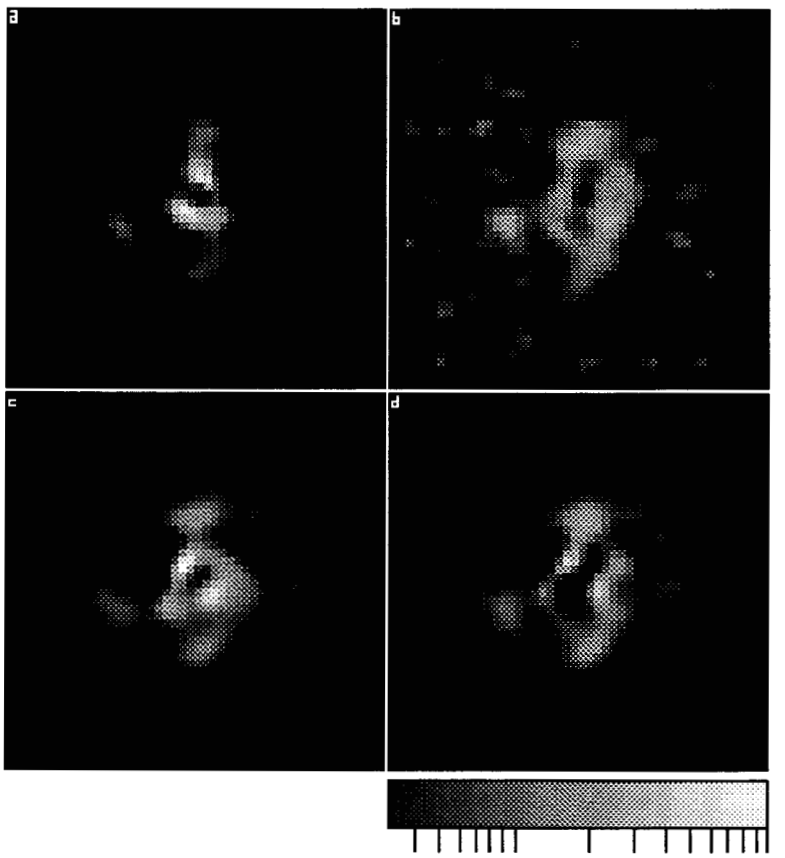

Fig. 4.— Tests of the fidelity of the subtracted/deconvolved images, as follows: (a) and (b) represent the results at 12.5 μm and 20.8 μm, respectively, using different PSFs than for Figure 3 (see text); (c) and (d) represent a comparison of the 20.8 μm results obtained on two separate days, i.e., June 13 and 14, respectively. All four images are presented on a 1.5-decade logarithmic scale, with a 6.″6 field of view.

4. Interpretation

The deconvolved images of α Sco at 12.5 μm can be characterized by a central ring of approximate radius 0.″3, surrounded by three discrete blobs at radial distances of about 1.″2 from the location corresponding to the central star. In the 20.8 μm images, the same three outer blobs are evident, but the structure of the inner emission is fainter and somewhat more complicated. We interpret these data as indicating the presence of two ejected shells, at radial distances of approximately 50 and 200 AU from the central star, with the outer shell containing three main condensations. Although we cannot exclude the possibility that the latter simply represent three peaks in a more continuous ring, they account for the majority of the observed flux density of the outer shell ($> 80\%$ at 12.5 μm and $> 50\%$ at 20.8 μm).

The observed radii, flux densities, and peak brightness temperatures of the two shells are listed in Table 1. The quoted uncertainties in the fluxes take account of photospheric subtraction errors. It is apparent that the 12.5/20.8 flux ratio for the inner shell is much larger than for the outer shell, as would be expected if the inner shell is at a higher temperature. Quantitatively, the flux ratios are consistent with dust temperatures in the range 200–600 K for the inner shell and > 800 K for the outer shell, depending on the assumed opacity law. Estimates of the dust mass, based on the data in this table and the expression given by Bloemhof & Danen 1995 and assuming small grains, indicate similar masses for the inner and outer shells, $\sim 4 \times 10^{-9}\, M_{\odot}$ each.

EDITOR: PLACE TABLE 1 HERE.

5. Discussion

Our conclusion that a substantial fraction (possibly one half) of the dust of α Sco is within a radial distance of $\sim$0.″3 from the star is in sharp contrast to previous investigations which have found that the inner $\sim$ 1″ is devoid of dust (Danchi et al. 1994, Bloemhof & Danen 1995) and suggests that there has been a relatively recent ejection. Our inferred inner shell is, however, consistent with the recent near-IR adaptive optics images of Cruzalèbes et al. (1998), which reveal the presence of several clumps close to the star, at distances of 0.″2, 0.″3, and 0.″4.

Our three outer blobs at 1.″2 are consistent with the shell reported by Bernat 1977 and Bloemhof & Danen 1995, now seen to be highly inhomogeneous. The fact that these blobs are all at about the same radial distance and yet are separated widely in azimuth suggests that the ejection process is regulated globally rather than locally. This might favor a pulsationally-driven ejection model, although there are some problems with the time scales involved. Specifically, if we assume a uniform outflow velocity of 17 km s^{-1} (from Bernat 1977, based on CO measurements), then the above shell radii imply an interval of about 45 years between successive ejections. This is much longer than the period, $\sim$ 6 years, of so-called "long-period" optical oscillations, assumed to represent the fundamental mode for radial pulsation (Smith et al. 1995). It is also difficult to reconcile the images with a convectively-driven ejection process, since a collection of uncorrelated convection cells would not produce a globally-organized shell structure unless there was some underlying regulation process such as a stellar activity cycle.

We thank the staff of the Keck Observatory for their support, and Dr. Michael Werner for helpful comments on the paper. The use of MIRLIN at the Keck Observatory was supported by an award from NASA's Origins program. Portions of this work were carried

out at the Jet Propulsion Laboratory, California Institute of Technology, under contract with the National Aeronautics and Space Administration. This research made use of NASA's Astrophysics Data System Abstract Service, and the Simbad database, operated at CDS, Strasbourg, France.

Table 1. Observed parameters of dust shells.

		Flux density [Jy]		Peak brightness temp. [K]	
Component	$r['']$	12.5 μm	20.8 μm	12.5 μm	20.8 μm
inner shell	0.3	437±30	76±17	207	122
outer shell	1.2	151±10	166±24	148	101

REFERENCES

Abbot, D. C., Telesco, C. M., & Wolff, S. C. 1984, ApJ, 279, 225

Bernat, A. P. 1977, ApJ, 213, 756

Bester, M., Danchi, W. C., Hale, D., Townes, C. H., Degiacomi, C. G., Mékarnia, D., & Geballe, T. R. 1996, ApJ, 463, 336

Bloemhof, E. E. & Danen, R. M. 1995, ApJ, 440, L93

Cruzalèbes, P., Lopez, B., Bester, M., Gendron, E. & Sams, B. 1998, A&A, 338, 132

Danchi, W. C., Bester, M., Degiacomi, C. G., Greenhill, L. J., & Townes, C. H. 1994, AJ, 107, 1469

Lucy, L. B. 1974, AJ, 79, 745

Monnier, J. D., Geballe, T. R., & Danchi, W. C. 1998 ApJ, 502, 833

Richardson, W. H. 1972, J. Opt. Soc. Am., 62, 55

Schwarzschild, M. 1975, ApJ, 195, 137

Smith, M. A., Teays, T. J. , Taylor, L. L. & Wasatonic, R. 1995, in R. S. Stobie & P. A. Whitelock, eds., Astrophysical Applications of Stellar Pulsation, ASP Conf. Series, Vol. 83, 403

Snow, T. P., Buss, R. H., Gilra, D. P., & Swings, J. P. 1987 ApJ, 321, 921

Tuthill, P. G., Haniff, C. A., & Baldwin, J. E. 1997, MNRAS, 285, 529

Walker, H. J. & Wolstencroft, R. D. 1988, PASP, 100, 1509

This manuscript was prepared with the AAS LaTeX macros v4.0.